Acta Acustica united with Acustica
Vol. 96 (2010) 168 – 178

Technical and Applied Papers
DOI 10.3813/AAA.918266

Digital Filters for Accurately Verifying the Performance of Hearing Protectors in Use

Annelies Bockstael[1,2], Dirk Deschrijver[3]*, Dick Botteldooren[1], Tom Dhaene[3], Bart Vinck[2]
Ghent University, Department of Information Technology, Acoustics[1] and IBBT[3],
Sint-Pietersnieuwstraat 41, 9000 Ghent, Belgium
Ghent University, Department of Oto-rhino-laryngology[2], De Pintelaan 185, 9000 Ghent, Belgium.
annelies.bockstael@ugent.be

Summary
The performance of hearing protectors can be assessed in situ by measuring the sound pressure inside the ear canal following the Microphone In Real Ear (MIRE) protocol. Thus a custom-made earplug has been designed with an inner bore, allowing the insertion of the MIRE measurement microphone. However, the actual exposure level can only be accurately predicted if the relationship, henceforth called transfer function, between the sound level at the microphone and at the eardrum is known. Previous research has revealed that the transfer function can be precisely approximated with an individualized FDTD model, but a simplified method is needed for practical implementation due to the time-consuming nature of this numerical technique. In this matter, a one-dimensional analytical model appears inadequate, hence an approximation to the detailed FDTD model based on digital filter design is proposed instead. Two different approaches have been applied to estimate the individualized filter coefficients: multiple linear regression and Multivariate Orthonormal Vector Fitting (MOVF). In general, both methods can predict an individual's transfer function quite accurately if the length of the earplug's inner bore and the length of the residual part of the ear canal behind the protector are known. However, MOVF seems more reliable for ears with a longer residual part.

PACS no. 43.66.Vt, 43.50.Hg

1. Introduction

Several studies clearly indicate that exposure to excessive noise is harmful to the auditory system [1]. In this regard, hearing protectors are often the most feasible solution to prevent occupational hearing loss [2].

Especially, custom-made earplugs deserve extra attention because they tend to be more positively rated with respect to usability and comfort [3].

One important issue is the noise dose received when wearing hearing protectors. The European Noise Directive on exposure limit values stipulates that the worker's effective exposure must take account of the attenuation provided by his hearing protectors [4]. Because of the well-known discrepancy between the attenuation measured in laboratory conditions and the real protection offered to an individual user [5], even custom-made hearing protectors merit individual field attenuation measurements [6].

Different procedures have been developed to assess hearing protectors in situ [7]. Among them, a Microphone In Real Ear (MIRE) based approach appears the most effective manner to conduct field measurements, yielding to the best trade-off between speed, accuracy, repeatability and correspondence with actual practice [8].

Thus, a custom-made earplug has been designed with an inner bore that allows the insertion of a miniature microphone registering sound pressure levels inside the ear canal behind the hearing protector [9]. In practice, this MIRE measurement microphone is mounted in a probe that also contains a reference microphone measuring the sound pressure outside the ear canal (see Figure 1).

The presence of the probe does not influence the attenuation of the earplug and measuring with this MIRE probe results in a very stable and reproducible outcome [10]. However, one critical issue is the manifest difference between the sound pressure level registered at the MIRE measurement microphone and the level of interest at the eardrum.

Previous research with a Head And Torso Simulator (HATS) has shown a stable and reproducible relation, henceforth called transfer function, between the sound pressure at the MIRE measurement microphone and at the the eardrum. Moreover, the measured transfer functions can be predicted with a Finite-Difference Time-Domain (FDTD) model of an ear canal occluded by an earplug [10]. Further investigation has revealed that the FDTD

Received 19 December 2008,
accepted 20 October 2009.

* D. Deschrijver is a postdoctoral research fellow of the Fund for Scientific Research Flanders (FWO-Vlaanderen).

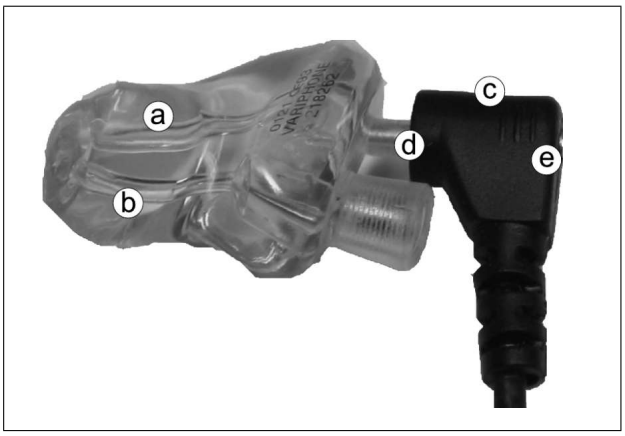

Figure 1. Earplug with two inner bores; one to adjust the attenuation (b) and the other test bore (a) for insertion of the MIRE probe (c) with measurement (d) and reference (e) microphone. The measurement microphone measures the sound level in the ear canal behind the hearing protector whereas the reference microphone registers the incoming sound level.

model of the HATS also accurately approximates the transfer functions for human ears if the most striking geometrical features of a particular ear and hearing protector are included in an individualized model [11]. The main features of the measurements and FDTD simulations are summarized in sections 2.1 and 2.2.

The numerically obtained transfer functions can be used to estimate the sound pressure at the eardrum from MIRE measurements. Although the model is well-suited in experimental and research settings, certain constraints make the practical implementation less feasible. First, detailed measurements of the geometrical parameters require specialized equipment and are time-consuming. Secondly, the computational cost for the FDTD model is quite large, making the incorporation in field measurement equipment nearly impossible. Hence a more simplified method is also needed.

Based on the relatively simple shape of the transfer function and the striking relationship with the morphology of earplug and ear canal, one might assume that a one-dimensional analytical model is sufficiently accurate to predict in practice the sound pressure at the eardrum. This approximation is elaborated in section 2.3, but the results distinctly show that the sound propagation under study is more complicated than can be captured in the analytical model.

To overcome this problem, a filter based approach is chosen instead because digital filters can easily be included in measurement equipment. In this matter, the FDTD transfer functions serve as a starting point to propose a set of filters suitable for estimating the sound pressure at the eardrum from measurements with the MIRE probe. Further, multiple linear regression (section 2.4) and Multivariate Orthonormal Vector Fitting (MOVF, section 2.5) are applied to predict for one specific ear the applicable filter by linking the filter characteristics to the most influential geometrical parameters of ear canal and earplug. Naturally, the aim is to achieve the right balance between the number of needed morphological variables – as few as possible – and the accuracy of the filter – as high as possible. In section 3, the outcome of the two approaches will be compared to the original FDTD simulations.

2. Material and methods

2.1. Measurements of the transfer function

Gaining insight in the fluctuation of sound pressure amplitude is the first step to build a numerical model. Therefore the sound pressure is simultaneously registered at the MIRE measurement microphone and at the eardrum for both a Head And Torso Simulator (HATS) and nineteen human subjects, all equipped with custom-made acrylic earplugs (see Figure 1). Measurements take place in an anechoic room to prevent disturbances from background noise or reverberation; all details can be found in [10] and [11].

The MIRE measurements are performed with a probe (see also Figure 1) containing a measurement and a reference microphone, namely two Knowles low noise FG-3652 microphones.

The HATS is a Brüel & Kjær HATS type 4128 C with ear simulator so that the sound can be registered at the place where anatomically the eardrum is found. When the custom-made earplugs are put in the HATS's outer ear canal, the sound pressure levels at the MIRE measurement microphone and at the eardrum can be measured simultaneously. Thus the transfer function under study (H_{me}) can be calculated directly by applying the following equation,

$$H_{me} = \sqrt{\frac{G_{me}(k)}{G_{mm}(k)} \cdot \frac{G_{ee}(k)}{G^*_{me}(k)}}, \qquad (1)$$

where H_{me} is the frequency response between MIRE measurement microphone (m) and eardrum (e), $G_{mm}(k)$ and $G_{ee}(k)$ are the autospectra, $G_{me}(k)$ is the cross-spectrum and $G^*_{me}(k)$ its complex conjugate.

Since the captured transfer functions should be absolutely independent of the test signal, the test space and the microphones, two reference free-field microphones are incorporated. All calibration steps are described in detail in previous work [10].

For the human subjects, a similar approach is followed by inserting an extra GN ReSound Aurical microphone in the outer ear canal. This device is designed to measure the sound pressure level at the eardrum and consists of a flexible silicone tube (outer diameter 0.85 mm) connected to an ear piece with microphone. The general approach is very similar to the measurements with the HATS and all details have been described previously [11]. One important remark is that the presence of the flexible silicone tube will not alter sound propagation in the outer ear canal an sich [12] but it does affect the attenuation of the earplug. This seems not critical since previous analyses have pointed out that changing the earplug's attenuation does not influence the transfer functions [10].

2.2. Finite-Difference Time-Domain model

2.2.1. Simulations of the transfer functions

In connection with the measurements, the sound pressure distribution in an ear canal occluded by an earplug is numerically simulated using the Finite-Difference Time-Domain (FDTD) technique. A key factor of this approach is that both pressure p and particle velocity $\mathbf{u}$ are discretised in Cartesian grids; more details can be found in [10]. This technique is chosen since the time domain method is both efficient and accurate and relies on a simple and straightforward concept. So it allows to calculate the transfer functions' spectra over the whole auditory spectrum at once [13].

The acoustically important features of ear canal and earplug are introduced in the model by boundary impedance of the form

$$Z = \mathrm{j}\omega Z_1 + Z_0 + \frac{Z_{-1}}{\mathrm{j}\omega}, \qquad (2)$$

which can be easily implemented in FDTD [14]. This means that for the ear canal the impedance of the ear canal's wall is included [15] to model sound propagation in the outer ear and in addition the acoustics of the middle and inner ear are represented by the impedance at the eardrum [16]. Further, the impedance of the MIRE microphone [17] is taken into account as well as the earplug's material [18] and the impedance of the entity earplug – ear canal [19].

Besides the impedance of the different structures, the effect of viscosity and heat conduction is included for the sound propagation in the earplug's channels because their diameter is very small. More detailed information about the FDTD model can be found in [10].

Apart from these general considerations, individual differences in ear canal and hearing protector might also mark the transfer functions. Therefore, the most striking geometrical features that are thought to influence sound propagation are accurately measured for each test subject and the HATS using either a caliper accurate up to 0.01 mm or a Coordinate-Measurement Machine (CMM) VM-250 Nexiv, manufactured by Nikon and accurate up to 0.1 μm. The parameters depicted in Figure 2 and 3 are included in the simulations with a 0.35 mm gridcell size and described in more detail in [11]. Naturally, the diameter of the earplug's channels is also taken into account, but not listed here because of its constant value amongst all hearing protectors.

2.2.2. Comparing measurements and FDTD-simulations

In Figure 4 an example of a measured and simulated transfer function is shown. In most cases, the resemblance between the simulated and the measured transfer functions is very satisfying [10, 11], yielding to the conclusion that the numerical simulations are a fair prediction of the transfer function between the sound level at the MIRE measurement microphone and at the eardrum. In this regard, the

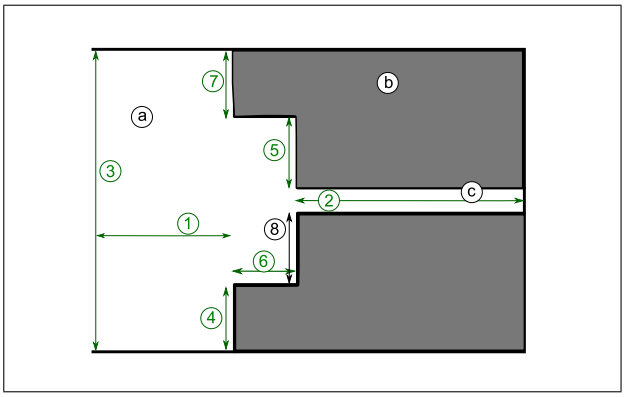

Figure 2. Individualized geometrical parameters for the FDTD simulations depicted on the vertical cross-section of the earplug in the ear canal taken through the test bore. The parameters in green (grey in b/w) serve as input variables for multiple linear regression carried out in section 2.4. a: ear canal, b: hearing protector, c: test bore; 1: length of residual part of the ear canal (l_1), 2: length of the test bore (l_2), 3: width of the hearing protector, 4: width of the lower rim of the hearing protector, 5: distance between the test bore and the upper rim of the hearing protector, 6: depth of the small pit at the end of the hearing protector, 7: width of the upper rim of the hearing protector, 8: distance between the test bore and the lower rim of the hearing protector.

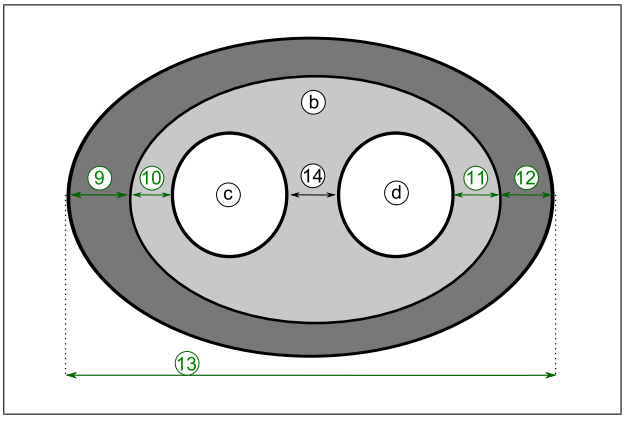

Figure 3. Individualized geometrical parameters for the FDTD simulations depicted on the horizontal cross-section of the earplug taken through the two inner bores at the part of the hearing protector nearest to the eardrum. The parameters in green (grey in b/w) serve as input variables for multiple linear regression carried out in section 2.4. b: hearing protector, c: test bore, d: second bore; 9: width of the left rim of the hearing protector, 10: distance between the test bore and the rim of the hearing protector, 11: distance between the second bore and the rim of the hearing protector, 12: width of the right rim of the hearing protector, 13: width of the hearing protector, 14: distance between the test bore and the second bore.

difference in the lower frequencies is related to the experimental setup [11] whereas the increased difference for frequencies above 6500 Hz is not considered critical [11].

All transfer functions appear to have the same global form with a distinct maximum between 2500 Hz and 3500 Hz and multiple minima above 4500 Hz; the most distinct minimum is often seen between 4500 Hz and

6500 Hz. Combining the results from measurements and the FDTD model for both the HATS and human subjects leads to the conclusion that the first maximum is most probably caused by resonance in the test bore with pressure peaking at the MIRE measurement microphone and appearing very low at the eardrum. Additionally, the most distinct minimum is most likely due to resonances in the residual part of the ear canal behind the hearing protector with pressure peaking at the eardrum but appearing low at the MIRE measurement microphone. Further, the measured transfer functions appear to be stable, reproducible and independent of the earplug's attenuation. The features of the transfer functions are discussed in more detail in [10] and [11].

Despite the common global shape, the intersubject variability appears to be substantial with respect to the exact frequency and amplitude of the extrema. This is little surprising given the relationship between the appearance of the transfer function and the particular structures of one's ear canal and hearing protector.

The FDTD simulations seem capable of capturing the link between geometrical characteristics and fluctuations in sound pressure amplitude, but are too time-consuming for implementation in practical measurement equipment. Therefore the knowledge from the FDTD model is used as starting point to develop three simplified approaches, described in the following sections, that could be used at the workfloor.

2.3. One-dimensional analytical model

In Figure 5 a schematic overview is drawn of an occluded ear canal, suitable for one dimensional modeling. In the simplified model viscothermal effects are neglected as well as the finite impedance of the earplug and ear canal material. Based on this approximations, the sound field in the microphone duct and in the residual ear canal can be approximated by plane waves traveling along the x-direction.

The specific acoustic impedance of the eardrum Z_t and the microphone impedance Z_m, both also included in the FDTD model, are used as boundary conditions. Continuity of pressure and particle velocity is imposed at the transition between the test bore and the ear canal ($x = l_1$).

These calculations give the following expression for the transfer function under study

$$\frac{p_{(l_1+l_2)}}{p_0} = \frac{S_1}{S_2}\frac{\left(-\frac{1+Z_m/\rho c}{1-Z_m/\rho c}+1\right)\mathrm{e}^{\mathrm{j}k(l_1+l_2)}}{-\frac{1+Z_t/\rho c}{1-Z_t/\rho c}+1} \cdot \frac{-\frac{1+Z_t/\rho c}{1-Z_t/\rho c}\mathrm{e}^{-2\mathrm{j}kl_1}-1}{-\frac{1+Z_m/\rho c}{1-Z_m/\rho c}\mathrm{e}^{2\mathrm{j}kl_2}-1}, \quad (3)$$

where p is the sound pressure, k the wave number, ρc the characteristic impedance, S_1 the cross-section of the ear canal and S_2 the cross-section of the test bore. Further $x = l_1 + l_2$ refers to the position of the MIRE measurement microphone and $x = 0$ of the eardrum; l_1, l_2, S_1 and S_2 can be adapted to establish individualized one-dimensional models analog to the FDTD models.

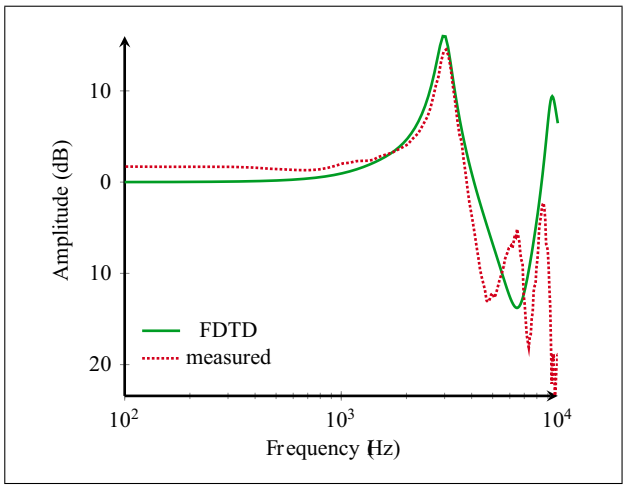

Figure 4. Example of similarity between simulation and measurement for one particular human ear: amplitude of the measured transfer function ('measured') and amplitude of the simulated transfer function ('FDTD').

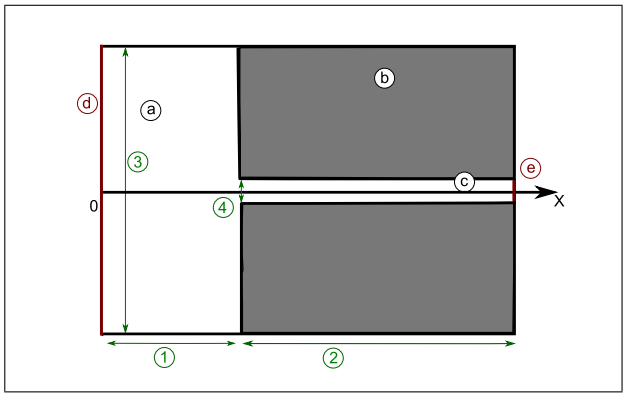

Figure 5. Schematic overview of the ear canal and test bore as included in the one-dimensional analytical approximation; pressure and particle velocity are calculated along the x-axis in the test bore and the residual part of the ear canal. a: ear canal, b: hearing protector, c: test bore, d: eardrum with impedance Z_t, e: MIRE measurement microphone with impedance Z_m; 1: length of residual part of the ear canal (l_1), 2: length of the test bore (l_2), 3: cross-section of the ear canal (S_1), 4: cross-section of the test bore (S_2).

Nevertheless, Figure 6 shows that the one-dimensional approach is over-simplified. The first maximum is elevated up to unrealistically high values and in addition shifted to higher frequencies, thus almost totally obscuring the minimum present in the measurements and FDTD model. This result is not entirely unexpected because certain assumptions made in the analytical approximation might not be completely fulfilled in reality.

First, the mass conservation equation or continuity equation might not be accurate at the transition between the test bore and the ear canal (at $x = l_1$) because the difference in diameter is large. In analytical models for Helmholtz resonators, an end correction is introduced to

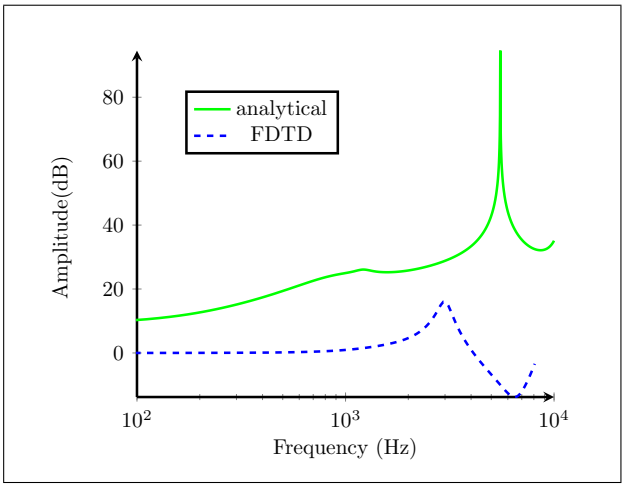

Figure 6. Example of dissimilarity between the one-dimensional analytical and the numerical approach for one particular human ear: amplitude for the transfer function obtained from the FDTD model ('FDTD') and the one-dimensional analytical model ('analytical').

take into account the near field of the flow field near the neck-end. This yields to replacing the length of the resonator neck by a (larger) effective length which would indeed shift the first maximum to lower frequencies.

Secondly, the continuity equation is not completely correct at small distances (compared to the wave length) from the transition. This means that the model is not adequate for small residual volumes because the wave front at the eardrum is no longer plane.

Thirdly, the viscothermal losses can not be neglected in ducts with small cross-section. The exponential damping can be introduced in the relation between wave number and frequency by including the absorption coefficient.

The above reasoning clearly shows that a relatively simple one-dimensional model has some obvious shortcomings. To handle this issue, it seems more efficient basing a simplified model on the accurate calculations of the FDTD simulations than introducing all the necessary corrections in the one-dimensional model.

2.4. IIR filter with coefficients obtained by multiple linear regression

2.4.1. Filter design

As described in section 2.2 FDTD simulations are carried out for nineteen subjects. Each simulation combines the general acoustical properties of an acrylic earplug and ear canal with individualized geometrical features. This approach yields to 37 different numerical models, one model per ear. In this matter, one ear is left out because the results obtained with the VM-250 Nexiv (see section 2.2) appeared to be erroneous.

In this section, the FDTD transfer functions are approached by IIR filters because digital filters, and especially FIR and IIR filters, can easily be included in measurement equipment. One of the standard methodologies for the design of such a filter is used; the complex frequency response of each simulated transfer function is approximated with a continuous-time transfer function being the quotient of two polynomials. If so desired, the fitted transfer function can be transformed into a discrete transfer function by applying a bilinear transformation.

To accomplish this, *invfreqs* from MATLAB (The MathWorks™) is used because this algorithm guarantees stability of the resulting linear system. The corresponding complex frequency response $H(s)$ can be written as

$$H(s) = \frac{B(s)}{A(s)} = \frac{b_{(1)}s^n + b_{(2)}s^{n-1} + \ldots + b_{(n+1)}}{a_{(1)}s^n + a_{(2)}s^{n-1} + \ldots + a_{(n+1)}}, \qquad (4)$$

with $s = \mathrm{j}2\pi f$, f representing the frequency.

The frequency range of interest is set between 0 Hz and 8000 Hz analogous to the frequencies tested with pure-tone audiometry [20]. Additionally, the filter coefficients are deliberately determined in the s-domain instead of the z-domain. In that way, the resulting filter can be digitalized afterward with a sampling frequency adapted to the sampling frequency of the measurement system used in practice. Finally, the order of $A(s)$ and $B(s)$ is chosen as low as possible, provided that the frequency response of the analogue filter $H(s)$ is almost identical to the FDTD simulated transfer function. It appears that this requirement is fulfilled if the order of both $A(s)$ and $B(s)$ is set at 6.

2.4.2. Linear regression for filter coefficients

The aim of the multiple linear regression analysis is finding a formal relationship between the coefficients of $H(s)$ and the geometrical variables of the ear canal and earplug. This way, an individual transfer function, resulting from an individualized filter, can be used in the measurement equipment to predict the sound pressure at the eardrum from the response of the MIRE measurement microphone without the need to perform a detailed FDTD simulation first. For stability reasons, linear regression will not be carried out with the coefficients of $A(s)$ and $B(s)$ but instead the poles and zeros, i.e. the roots of respectively $A(s)$ and $B(s)$, serve as dependent variables.

Dependent variables For most ears, only the first and second zero appear to be real, all other poles and zeros are complex. For the latter, the real and the imaginary part are fitted separately using linear regression. Because all coefficients in Equation 4 are real, the complex conjugate of each complex pole or zero is also a pole or zero of the filter under study. In that case, only the real and imaginary part of the pole/zero with a positive imaginary part are considered for the regression analysis. The corresponding complex conjugate can then be easily deduced from the resulting formulas.

Independent variables The possible independent variables of the linear regression are the geometrical parameters seen in both cross-sections of the earplug and ear canal, depicted in green (grey in b/w) in Figure 2 and 3. Linearly dependent variables are omitted.

Building the regression model All statistical analyses are carried out with the statistical software R. Based on scatter plots and Pearson correlation coefficients between dependent and independent variables, a manual step-forward regression procedure is followed. This means that one independent variable is added at the time, starting with the variable that shows both graphically and numerically the strongest linear correlation with the dependent variable. The procedure is repeated until the adjusted R^2 equals or exceeds 0.80. When extra independent variables are added, care is taken that they are not correlated to the variables that are already included in the model and that there are always 6 to 10 observations per variable included in the regression model [21].

A manual stepwise approach is preferred over an automatic procedure because the practical feasibility has to be taken into account. This means that geometrical parameters that can be measured more easily are preferred as independent variables, as long as they yield to accurate predictions.

Checking the underlying assumptions Before the obtained models are actually used to predict the poles and zeros for a particular transfer function, the aptness of the assumptions of linear regression are checked first [21].

The assumptions that the residuals come from a normal distribution is verified with the Kolmogorov-Smirnov test and the Shapiro-Wilk normality test. If the distribution of the residuals is far from normal ($p < 0.01$), the regression model is reconsidered. Further, the random distribution of studentized residuals around zero is visually assessed by drawing a scatter plot. Because left and right ears of the same subject are included, possible autocorrelation between the residuals is examined by calculating the Durban Watson statistic.

Outliers and influential observations are detected by computing the Mahalanobis distance, the df-betas, the Cook's distance and the leverage. The Mahalanobis distance measures the influence of a case i on the fitted value $\hat{Y}_i$ whereas the Cook's distance considers the influence of the ith case on all n fitted values. Subsequently, the df-beta measures the influence of the ith case on each regression coefficient. Finally, the leverage measures the difference between the vector of the ith observations of the independent variable and the vector of means of all independent variables [21]. The values of influential observations are carefully inspected and action is undertaken whenever necessary.

2.4.3. Numerical results

For the real part of the first pole ($\Re(p1)$), the real ($\Re(p3)$) and imaginary ($\Im(p3)$) part of the third pole and the imaginary part of the fifth pole $\Im(p5)$, the regression models could be established without any problems, including all observations of the dataset. The resulting models are summarized in Table I, revealing that only the length of the test bore l_2 and the length of the residual part of the ear canal l_1 are needed as independent variables. For all the linear models, both normality tests yield to insignificant p-values ($p > 0.01$). Furthermore, none of the values of influential observations are unlikely nor is there reason to believe that they have been measured incorrectly.

For the real part of the fifth pole ($\Re(p5)$) and zero ($\Re(z5)$), the adjusted R^2 does not reach 0.80. Since adding more variables apart from l_1 and l_2 does not substantially increases this value and since the residuals of the model are normally distributed, the most simple model with the highest adjusted R^2 is chosen at least if the adjusted R^2 approximates 0.80. This reasoning is also followed in the subsequent analysis.

For the imaginary part of the first pole ($\Im(p1)$), the real part of the fifth pole ($\Re(p5)$), the real ($\Re(z3)$) and the imaginary ($\Im(z3)$) part of the third zero and the imaginary part of the fifth zero ($\Im(z5)$), the Shapiro-Wilk test yields to a significant p-value ($p < 0.01$) due to one – two in case of $\Re(z3)$ – more extreme error term. In these cases, the following rule of thumb is applied. Since none of the simulated transfer functions or corresponding filters shows any manifest errors, the influence of the observation in question on the resulting regression is calculated. If the inclusion of the observation only influences the corresponding fitted value of this particular observation, this observation is kept. However, if the Cook's distance of this observation exceeds 1 or if the df-beta exceeds $\frac{2}{\sqrt{n}}$ with n the number of observations (37) the regression analysis is carried out without the observation in question [21]. The resulting models are also summarized in Table I.

For the first and second zero, the regression analysis becomes much more complicated because most ears have real first and second zeros, but a distinct minority has complex first zeros. The complex zeros tend to be associated with longer ear canals although this relationship is not absolute. Additional FDTD simulations with higher values for l_1 and the total range of values for the other parameters reveal that the combination of a longer ear canal with a shorter test bore and a deeper pit at the end of the earplug tends to influence the spectrum of the transfer function. Actually, those simulations show more often a (very) slight minimum in the lower frequency region whereas most transfer functions rise monotonically in these frequency range or remain constant. The extra minimum explains why the zeros of the corresponding filter differ from the majority. Unfortunately, the emergence of this minimum can not be absolutely predicted based on the geometrical parameters, hence it is not feasible to make different regression models for both groups. Because of the nature of the problem, it is also very unlikely that filters with higher orders for the numerator will solve this problem.

Given the limited number of ears resulting in complex first zeros, only the real zeros are used for linear regression. Naturally, this implies that the regression model is less accurate for higher values of l_1. The results for the real part of the first ($\Re(z1)$) and second ($\Re(z2)$) zero are also reported in Table I.

The Durbin Watson statistic does not suggest autocorrelation for any of the tabulated models ($\alpha = 0.05$).

Table I. Summarized statistics for linear regression tabulating for each dependent variable ('dep'), the predictive independent variables ('idep') with l_1 (in metre) the length of the residual part of the ear canal and l_2 (in metre) the length of the test bore; 'inter' stands for the intercept of the function. Further, the corresponding coefficients ('coefficients') are listed for each variable together with their p-value 'p'. Finally, the adjusted R^2 is given (aR^2) and the case numbers of the observations that are not included in the model ('rejected'), where 'cp' refers to the cases with complex zeros.

dep	idep	coefficients	p	aR^2	rejected
$\Re(p1)$	(inter)	$2.3 \cdot 10^4$	< 0.05	0.89	none
	l_1	$-2.6 \cdot 10^7$	< 0.001		
	l_2	$-0.8 \cdot 10^6$	< 0.05		
	$l1 \cdot l2$	$0.9 \cdot 10^8$	< 0.01		
$\Im(p1)$	(inter)	$11.6 \cdot 10^4$	<0.001	0.89	none
	l_2	$-2.3 \cdot 10^6$	<0.001		
$\Re(p3)$	(inter)	$-20.2 \cdot 10^2$	< 0.001	0.98	none
	l_2	$25.3 \cdot 10^3$	< 0.001		
$\Im(p3)$	(inter)	$37.9 \cdot 10^3$	< 0.001	0.99	none
	l_2	$-7.5 \cdot 10^5$	< 0.001		
$\Re(p5)$	(inter)	$-10.4 \cdot 10^3$	< 0.001	0.74	none
	l_1	$0.5 \cdot 10^5$	< 0.001		
	l_2	$1.7 \cdot 10^5$	< 0.001		
$\Im(p5)$	(inter)	$12.2 \cdot 10^3$	< 0.001	0.84	none
	l_1	$7.0 \cdot 10^4$	< 0.001		
	l_2	$-4.0 \cdot 10^4$	< 0.001		
$\Re(z1)$	(inter)	$-0.9 \cdot 10^6$	< 0.001	0.92	20 + cp
	l_1	$0.9 \cdot 10^7$	< 0.001		
	l_2	$3.8 \cdot 10^7$	< 0.001		
	$l1 \cdot l2$	$-3.6 \cdot 10^9$	< 0.001		
$\Re(z2)$	(inter)	$-0.8 \cdot 10^5$	<0.001	0.81	cp
	l_1	$-3.5 \cdot 10^6$	< 0.001		
	l_2	$2.9 \cdot 10^6$	< 0.001		
$\Re(z3)$	(inter)	$-8.2 \cdot 10^3$	< 0.001	0.85	29 + 23
	l_1	$2.1 \cdot 10^5$	< 0.001		
$\Im(z3)$	(inter)	$0.5 \cdot 10^5$	< 0.001	0.83	29
	l_1	$-2.6 \cdot 10^6$	< 0.001		
	l_2	$0.9 \cdot 10^6$	< 0.05		
$\Re(z5)$	(inter)	$-10.5 \cdot 10^3$	< 0.001	0.75	none
	l_1	$0.6 \cdot 10^5$	< 0.001		
	l_2	$1.6 \cdot 10^5$	< 0.001		
$\Im(z5)$	(inter)	$12.7 \cdot 10^3$	< 0.001	0.88	19
	l_1	$9.5 \cdot 10^4$	< 0.001		
	l_2	$-0.6 \cdot 10^5$	< 0.001		

To sum up, inclusion of only the length of the residual part of the ear canal (l_1) and/or the length of the test bore (l_2) in the regression models appears sufficient to make reasonably accurate predictions. This clearly enhances the suitability of this approach in practice because these parameters can be measured easily, quickly and accurately for each individual.

2.5. Multivariate orthonormal vector fitting

Although the linear regression provides good results for most poles and zeros, there are several shortcomings. First, the resulting equations are not entirely valid for the longest ear canals. Secondly, not all observations could be included in all models and thirdly, estimating the real and imaginary part of each pole and zero separately might increase the overall error. Therefore, an alternative approach is also used, namely the Multivariate Orthonormal Vector Fitting (MOVF) algorithm. Whereas multiple linear regression aims to fit the trajectories of each pole and zero separately, this approach computes an accurate multivariate model that describes the configuration of the poles and zeros as a whole. The overall goal of the MOVF algorithm is the same as for the linear regression; establishing a parameterized rational model that simplifies to an individualized frequency-dependent transfer function for certain values of the independent variables. The details of this approach are described in [22], a short outline of the modeling procedure is given here for convenience of the reader.

2.5.1. Model representation

Because the regression analysis has clearly shown that the length of the ear canal (l_1) and the length of the test bore (l_2) are the most influencing variables, the MOVF algorithm computes a rational trivariate model $R(s, l_1, l_2)$ that has the frequency variable s (recall $s = j\omega$), but also l_1 and l_2 as parameters. It is defined as the ratio of a parameterized numerator $N(s, l_1, l_2)$ and denominator $D(s, l_1, l_2)$.

$$R(s, l_1, l_2) = \frac{N(s, l_1, l_2)}{D(s, l_1, l_2)} = \frac{\sum_{p=0}^{P} \sum_{v_1=0}^{V_1} \sum_{v_2=0}^{V_2} c_{p,v_1,v_2} \left(\phi_p(s) \varphi_{v_1}(l_1) \varphi_{v_2}(l_2)\right)}{\sum_{p=0}^{P} \sum_{v_1=0}^{V_1} \sum_{v_2=0}^{V_2} \tilde{c}_{p,v_1,v_2} \left(\phi_p(s) \varphi_{v_1}(l_1) \varphi_{v_2}(l_2)\right)}. \quad (5)$$

The frequency-dependent basis functions $\phi_p(s)$ are orthonormal rational functions that are based on a prescribed set of poles $\vec{a}$. These poles $\vec{a}$ are chosen as stable complex conjugate pairs with small negative real parts and imaginary parts linearly spaced over the frequency range of interest. The parameter-dependent basis functions $\varphi_{v_1}(l_1)$ and $\varphi_{v_2}(l_2)$ are also rational functions that are chosen in partial fraction form as a function of jl_1 and jl_2. They are based on a prescribed set of poles $\vec{b}_1$ and $\vec{b}_2$ respectively, which are chosen as complex pairs with small real parts of opposite sign and imaginary parts linearly spaced over the parameter ranges. A linear combination of two partial fractions is formed to ensure that they constitute a real function. The variables P, V_1 and V_2 denote the number of basis functions, and are chosen according to the dynamic behavior (i.e. the order) of each variable independently.

2.5.2. Calculation of model coefficients

Based on the FDTD simulations that are performed in section 2.2, a dense set of data samples $\{(s, l_1, l_2)_k, H(s, l_1, l_2)_k\}_{k=1}^{K}$ is obtained, taking into account the length of a particular test bore and ear canal. For the other

geometrical parameters, the average values from the original dataset are chosen since the regression analysis has shown that in general their influence on the resulting transfer function is small. The goal of the MOVF algorithm is then to estimate the optimal values of the coefficients c_{p,v_1,v_2} and $\tilde{c}_{p,v_1,v_2}$ of the trivariate transfer function in such a way that it approximates the data samples in a least square sense. A linear approximation to this nonlinear optimization problem is obtained by using an iterative procedure called the Sanathanan-Koerner iteration [23]. In the first iteration step ($t = 0$), Levi's cost function is minimized to obtain an initial guess of the model coefficients. In successive iteration steps ($t = 1, ..., T$), updated values of the model coefficients are found by using the previously estimated denominator as an inverse weighting to the least-squares equations ($D^{(0)} = 1$).

$$\min_{c^{(t)},\tilde{c}^{(t)}} \sum_{k=0}^{K} \left| \frac{N^{(t)}(s,l_1,l_2)_k}{D^{(t-1)}(s,l_1,l_2)_k} - \frac{D^{(t)}(s,l_1,l_2)_k}{D^{(t-1)}(s,l_1,l_2)_k} H(s,l_1,l_2)_k \right|^2 \tag{6}$$

This process is repeated in an iterative way until all the model coefficients have converged. To improve the convergence properties of the iteration, a relaxed non-triviality condition is applied. It is also noted that the trivariate model reduces to a regular, univariate transfer function for fixed values of l_1 and l_2.

2.5.3. Numerical results

To build the trivariate MOVF model, 100 FDTD simulations are performed, based on a grid of 10 × 10 values which are equidistantly spread over the parameter ranges of l_1 ([0.008 m - 0.0212 m]) and l_2 ([0.0212 m - 0.0284 m]). For each FDTD model, 97 equidistant frequency samples are calculated from 0 Hz up to about 8000 Hz. This data is used by the MOVF algorithm to compute a parameterized macromodel. If the number of poles is set to 2 (l_1), 6 (l_2) and 8 (s), then good agreement is found between the MOVF model and the data. The optimal values of the model's coefficients (378) are depicted in Figure 7.

An overall assessment of the model quality is acquired by comparing the response of the MOVF model with a dense set of validation samples. It is found that the RMS error of the approximation model is equal to 2×10^{-3} ,which corresponds well to the desired accuracy. As an illustration, the model response for a test bore with length 0.0247 m is visualised in Figure 8.

3. Comparison of multiple linear regression and MOVF models

Because of the obvious shortcomings of the one-dimensional analytical model, these predictions are no further considered. To compare the linear regression and MOVF directly, the expected transfer functions are calculated in MATLAB for each of the 37 ears in the original dataset.

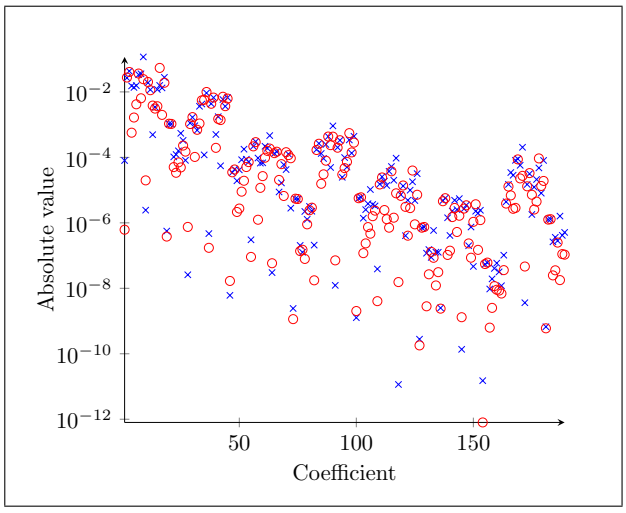

Figure 7. The optimal values of the MOVF model's coefficients with the values of c_{p,v_1,v_2} indicated by '×' and the values of $\tilde{c}_{p,v_1,v_2}$ by 'o'.

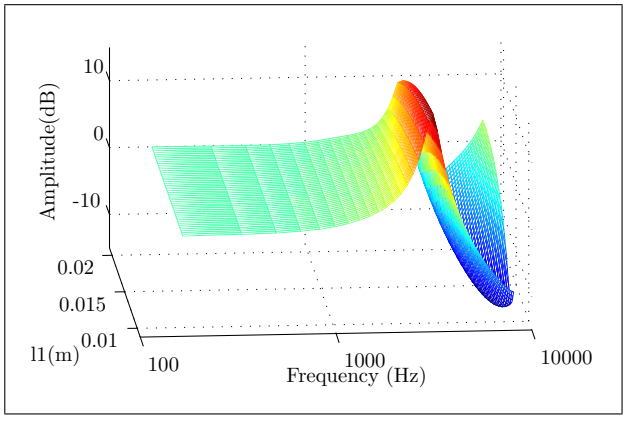

Figure 8. Example of the validation data samples for the three-dimensional MOVF model for a test bore with length 0.0247 m.

Worthwhile to mention is the fact that the actual computer time is acceptable for both approaches. The fitted transfer functions are then compared to the original simulations, because – although relying on two different fitting principles – they all aim to approach the FDTD transfer functions as accurately as possible.

In general, both models do well for ear canals of moderate length, an example is seen in Figure 9a. However, the MOVF approach clearly improves the prediction made by the linear regression model for more extreme lengths of the ear canal (see Figure 9b). This graphic also reveals that for this particular case, the prediction of the MOVF model is somewhat less accurate for the transfer function's minimum in the higher frequencies. The small deviation is not caused by an inaccurate fitting of the data, but it is connected with the fact that the FDTD simulations (which are used to compute the MOVF model) are based on average values for all geometrical parameters, except for the length of the test bore and ear canal. Although the influence of the other geometrical parameters is small, they still might affect the transfer functions. Nevertheless, they are not in-

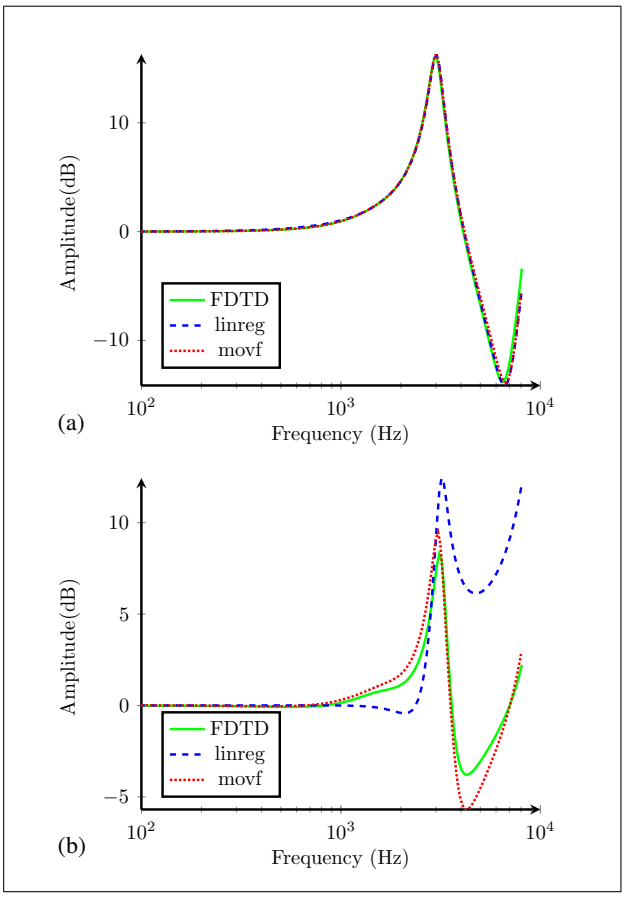

Figure 9. Comparison between the simulated transfer function ('FDTD') and the transfer function fitted with linear regression ('linreg') or MOVF ('movf'). Residual ear canal length: (a) 0.0120 m, (b) 0.0203 m.

cluded in the FDTD simulations for the MOVF and hence their influence cannot be included by this model. However, the resulting inaccuracy is not critical because previous research has shown that the exact transfer function's minimum is not unambigiously specified since it strongly depends on the position of the earplug in the ear canal [11].

To quantify the possible improvements between the fitted models, the difference is taken between the magnitude of the FDTD simulated transfer functions of the original data set and the magnitude of respectively the transfer function fitted with linear regression and with MOVF. Then, this difference is squared and summed over four clearly distinguishable frequency ranges, i.e. between 100 Hz and 1500 Hz where most functions are either constant or monotonically rising; between 2500 Hz and 4000 Hz where a distinct maximum is seen; between 4500 Hz and 6500 Hz including a clear minimum and finally between 6500 Hz and 8000 Hz where most functions are again rising. Finally, the sums are divided by the number of frequency points to make the quadratic errors comparable across the different frequency ranges. The quadratic errors are compared between the models with a Wilcoxon signed-rank test instead of a paired student t-test

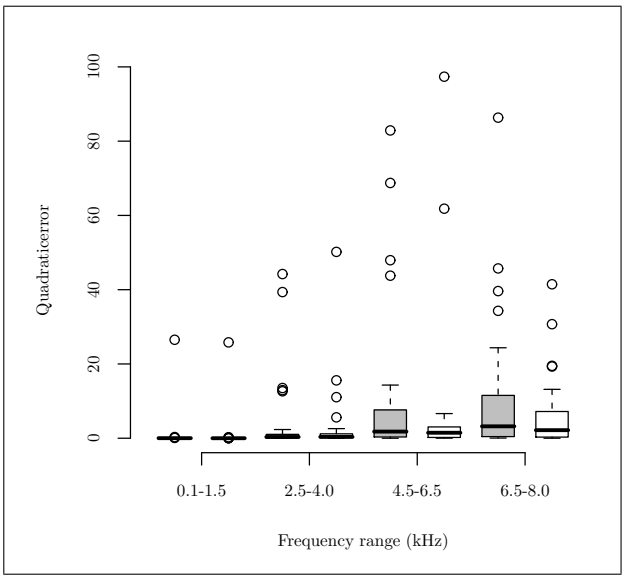

Figure 10. Quadratic error for corresponding transfer functions estimated from multiple linear regression compared to the FDTD models (gray) and estimates from the MOVF models compared to FDTD models (white), calculated for the frequency region from 0.1 kHz to 1.5 kHz, from 2.5 kHz to 4.0 kHz, from 4.5 kHz to 6.5 kHz and from 6.5 kHz to 8.0 kHz. The boxes span the middle half of the ordered observations and the thick black lines inside represent the median. The whiskers extend to the most extreme data point which is no more than 1.5 times the interquartile range from the boxes. The circles represent data points that fall outside these limits.

Table II. The quadratic error between corresponding transfer functions estimated from multiple linear regression and from the FDTD models is statistically compared to the quadratic error between the estimates from the MOVF models and from FDTD models. The p-values are tabulated per frequency range for the Wilcoxon signed-rank test (Wilcoxon test).

Frequency range	Wilcoxon test
0.1 kHz–1.5 kHz	<0.001
2.5 kHz–4.0 kHz	0.80
4.5 kHz–6.5 kHz	0.19
6.5 kHz–8.0 kHz	0.38

because the data tend to be right-skewed and there are not enough observations to apply the central limit theorem.

For the lower frequency region, MOVF performs clearly better ($p < 0.001$), but the error is already quite small in this range. For the other frequency regions, no unambiguous statistical differences are found (see Table II). Nevertheless, it is important to notice that the quadratic error always tends to be lower for the MOVF approach (see Figure 10) and that cases of total mismatch of the linear regression fit (see Figure 9b) are never seen for MOVF.

4. Discussion

Previous research has demonstrated that the MIRE method is a suitable way to measure the performance of hearing

protectors in situ [8]. Further, the sound pressure at the eardrum can be accurately predicted from the response of the MIRE measurement microphone provided that the transfer function is known. Especially in the frequency region below 6000 Hz, the measured transfer functions and the transfer functions predicted from the FDTD model are in good agreement [10].

Overall, the global shape of the obtained transfer functions is relatively simple and can be clearly traced down to the main features of test bore and ear canal. These findings might question the need for the quite complicated numerical FDTD simulations and the extensive regression and MOVF models, especially when it comes to practical implementation. Conversely, the sound pressure distribution in the occluded ear canal could be approximated with a one-dimensional analytical model.

However, section 2.3 clearly reveals that a basic one-dimensional analytical approach is not useful to predict the sound pressure at the eardrum from measurements by the MIRE microphone. Inclusion of viscothermal losses – for instance in the test bore – seem indispensable as is the extension to at least a two-dimensional model so that acoustically important features like the earplug's pit can be included. In theory, problems could to a certain extend be solved by adding suitable correction terms, but numerical techniques seem more efficient and straightforward.

Hence, the simulated transfer function are approximated with a filter approach. The advantage of this procedure is that the acoustical mechanisms included in the FDTD simulations still play their part because the filter characteristics are directly related to the simulated transfer functions. In addition, the filter coefficients can be linked to specific geometrical features of ear canal and earplug with multiple linear regression and MOVF. The thus found expressions only need the length of the ear canal and the test bore to predict new transfer functions. The total length of the ear canal can easily be measured by sliding a silicone tube into the ear canal, for example at the time that the ear impression for the custom-made earplug is taken. The length of the earplug itself and of its inner bore can be determined during the manufacturing process.

The filters based on linear regression and MOVF perform both well with rather marginal statistical differences. However, it must be noted that the linear regression model is actually based on the original FDTD data set that is also used to calculate the quadratic error, whereas the MOVF starts from a dense set of new simulations (see section 2.5.2). This might artificially lower the quadratic error for the linear regression model. Moreover, the MOVF performs clearly better for cases where a longer ear canal is combined with a shorter test bore.

Determining the sound pressure level at the eardrum provides insight in the performance of a hearing protector, but it does not have to be an end point. From the level at the eardrum, the insertion loss and the noise reduction can be derived. In this matter, the insterion loss is defined as the difference between the sound pressure level before and after noise treatment, i.e. with and without a hearing protector in place. The noise reduction is the difference between the sound pressure outside the ear canal and inside behind the hearing protector [24]. For these calculations, the sound pressure at the eardrum has to be combined with head-related-transfer-functions (HRTF) [7]. Research suggests that an individual's HRTF can be approximated by average values [25, 7], but th is will nevertheless increase uncertainty especially for the higher frequencies. Therefore, further research could focus on the practical feasibility and implementation of individualized HRTFs.

5. Conclusion

This paper proposes a practical method for determining the individualized sound pressure level at the eardrum when using the MIRE technique to evaluate the performance of hearing protectors. It is based on measurements of the sound pressure level at a microphone embedded in the HPD and only two individual morphological parameters: the length of the test bore where the measurement microphone resides and the length of the residual portion of the ear canal behind the protector.

In this paper three models for the transfer function between eardrum and measurement microphone are compared. First, a basic one-dimensional analytic model proved to be insufficient. Further, two other models that are based on fitting rational digital filters on detailed simulations – previously proved to be quite accurate – both seem to perform sufficiently well.

The first method starts from fitting a linear model to obtain the filter coefficients from the two lengths mentioned above. It has the advantage of simplicity and limited number of coefficients but is slightly less accurate. The second method, a multivariate orthonormal vector fitting, is more generally applicable in a sense that it also allows to find the transfer function for more extreme ear dimensions. However, the number of coefficients it uses is much more elaborate.

Both filter approximations provide the filters in virtually no time - that is compared to a full numerical simulation - and thus can be implemented in a practical measurement system.

Acknowledgement

This work was partly supported by the Fund for Scientific Research Flanders (FWO-Vlaanderen).

References

[1] M. Śliwinska-Kowalska, P. Kotylo: Evaluation of individuals with known or suspected noise damage to hearing. Audiological Medicine **5** (2007) 54–65.

[2] P. M. Arezes, A. S. Miguel: Hearing protectors acceptability in noisy environments. Ann. Occup. Hyg. **6** (2002) 531–536.

[3] R. Neitzel, S. Somers, N. Seixas: Variability of real-world hearing protector attenuation measurements. Ann. Occup. Hyg. **50** (2006) 679–691.

[4] Directive 2003-10-EC on the minimum health and safety requirements regarding the exposure of workers to the risks

arising from physical agents (noise). Brussels, 2003, European Parliament and Council.

[5] J. Franks: Comparison of the regulatory noise reduction rating (NRR) and the required ANSI S3.19 test method with real world outcomes and results from testing with the new ANSI S12.6B method. Workshop on hearing protector devices, Washington DC, March 2003, United States Environmental Protection Agency.

[6] E. H. Berger, J. R. Franks, F. Lindgren: International review of field studies of hearing protection attenuation. New York, 1996, A. Axlesson, R. P. Borchgrevink, R. P. Hamernik, P. Hellstrom, D. Henderson, R. J. Salvi (eds.), Thieme Medical Pub, 361–377.

[7] J. G. Casali, D. W. Mauney, B. J. Alton: Physical vs. psychophysical measurements of hearing protection attenuation - a.k.a. MIRE vs. REAT. Sound Vib. (July 1995) 20–27.

[8] E. H. Berger, J. Voix, R. W. Kieper: Methods of developing and validating a field-mire approach for measuring hearing protector attenuation. Spectrum, Savannah GA, February 2007, 32nd Annual Conference of the National Hearing Conservation Association.

[9] J. Voix: Mise au point d'un bouchon d'oreille 'intelligent' (Development of a 'smart' earplug). Dissertation. Ecole de Technologie Supérieure Université du Québec, june 2006.

[10] A. Bockstael, B. de Greve, T. Van Renterghem, D. Botteldooren, W. D'haenens, H. Keppler, L. Maes, B. Philips, B. Vinck: Verifying the attenuation of earplugs in situ: method validation using artificial head and numerical simulations. J. Acoust. Soc. Am. **124** (2008) 973–981.

[11] A. Bockstael, T. Van Renterghem, D. Botteldooren, W. D'haenens, H. Keppler, L. Maes, F. Swinnen, B. Philips, B. Vinck: Verifying the attenuation of earplugs in situ: method validation on human subjects including individualized numerical simulations. J. Acoust. Soc. Am. **125** (2009) 1479–1489.

[12] P.-A. Hellstrom, A. Axelsson: Miniature microphone probe tube measurements in the external auditory canal. J. Acoust. Soc. Am. **93** (1993) 907–919.

[13] T. Van Renterghem: The finite-difference time-domain method for simulation of sound propagation in a moving medium. Dissertation. Ghent University, 2004.

[14] D. Botteldooren: Finite-difference time-domain simulation of low-frequency room acoustic problems. J. Acoust. Soc. Am. **98** (1995) 3302–3308.

[15] H. P. Wit, K. J. Damme, C. W. Van Spoor: Fysica voor de fysiotherapeut (physics for the physiotherapist). Bunge, Utrecht, 1987.

[16] M. Kringlebotn: Network model of the human middle ear. Scandinavian Audiology **17** (1988) 75–85.

[17] Microphone handbook. Brüel & Kjær, July 1996.

[18] L. Hillström, M. Mossberg, B. Lundberg: Identification of complex modulus from measured strains on an axially impacted bar using least squares. J. Sound Vib. **230** (2000) 689–707.

[19] P. Hiselius: Attenuation of earplugs - objective predictions compared to subjective REAT measurements. Acta Acust. United Ac. **91** (2005) 764–770.

[20] Acoustics - audiometric test methods - part 1: Basic pure tone air and bone conduction threshold audiometry. International Standard Organisation, ISO 8253-1:1989, 1989.

[21] M. H. Kutner, C. J. Nachtscheim, J. Neter, W. Li: Applied linear statistical models. 5th ed. McGraw-Hill, New York, 2004.

[22] D. Deschrijver, T. Dhaene, D. De Zutter: Robust parametric macromodeling using multivariate orthonormal vector fitting. IEEE Trans. Microw. Theory Tech. **56** (2008) 1661–1667.

[23] C. K. Sanathanan, J. Koerner: Transfer function synthesis as a ratio of two complex polynomials. IEEE Trans. Autom. Control **8** (Januari 1963) 56–58.

[24] E. H. Berger: Preferred methods for measuring hearing protector attenuation. Environmental noise control, Brazil, August 2005, Inter Noise.

[25] D. Hammershøi, H. Møller: Determination of noise immission from sound sources close to the ears. Acta Acust. United Ac. **94** (2008) 114–129.